Acta Mechanica Solida Sinica (2023) 36:603–611
https://doi.org/10.1007/s10338-023-00409-9

Vortex Evolution Behavior in Self-Assembly of Flow Units in Metallic Glasses

Jie Lian[1,2] · Ruyue Song[1,2] · Yan Chen[1,2] · Lanhong Dai[1,2]

Received: 23 May 2023 / Revised: 9 June 2023 / Accepted: 11 June 2023 / Published online: 11 July 2023

Abstract
Shear banding in amorphous metals originates from the activation and percolation of flow units. To uncover the self-assembly dynamics of flow units in metallic glasses, a rectangular sample with two flow units embedded in the matrix undergoing simple shearing was analyzed using finite element simulations. The vortex evolution behavior, including activation, growth, and collapse during the self-assembly of flow units, was revealed. It was found that the formation of a mature vortex indicates the onset of yielding, and the collapse of the vortex represents the percolation of flow units or shear localization. The effects of initial free volume distribution and the distance between flow units on vortex behavior were also studied. Increasing the initial free volume concentration within flow units or the matrix leads to a gentler vortex evolution process and better homogeneous plasticity. The shape of vortex tends to be "flatter" with the increase in flow units' spacing, and the optimal spacing was found to maximize the strength of the material.

Keywords Vortex · Free volume · Self-assembly · Flow units · Metallic glasses

1 Introduction

Different from the traditional crystalline metals, the plastic deformation of which is accommodated by dislocation, metallic glasses deform plastically by the movement of atomic clusters which range in size from a few to a few hundred atoms, termed shear transformation zones (STZs) or flow units [1–4]. Experimental observations tell that metallic glasses exhibit intrinsic structural and dynamic inhomogeneity, which are composed of hard regions surrounded by soft regions [5–7]. The local heterogeneities, which depend on the thermal and mechanical history of metallic glasses, contain the secret of structural origin of the deformation behavior [8–11]. As an initial deformation zone, the flow units can be activated and self-assemble by applied stress or elevated temperature, leading to the formation of a shear band [12–16]. Since shear bands in metallic glasses have a characteristic thickness of ~10 nm [17, 18], and the dynamic process of their formation is so fast [19], it is extremely difficult to study the self-assembly behavior of flow units experimentally [20]. Therefore, research on this critical issue has so far relied on theoretical analysis and molecular dynamics simulation [13, 21–26].

Earlier simulations indicate that flow units behave as Eshelby inclusions, which induce quadrupolar elastic displacements in the surrounding materials and arouse density variations in shear bands [21, 24]. Because of these long-range interactions between elastic fields, flow units are not independent, random events may start percolating along the direction of maximum shear stress, and eventually, a shear band forms [12, 19, 22, 27, 28]. Şopu et al. proposed a two-unit mechanism of catalytic self-assembly of STZs through identifying the structural perturbation generated by an STZ in the surrounding matrix and tracing how such a perturbation triggers the activation of the neighboring STZ [13]. Recently, Yang et al. demonstrated that shear band formation results from the operative manipulation of shear-dominated zones, dilatation-dominated zones, and rotation-dominated zones [16]. The autocatalytic generation of successive strong strain and rotation fields was observed in the self-assembly of flow units, where a "vortex"-like flow plays a critical role [13, 16].

✉ Yan Chen
chenyan@lnm.imech.ac.cn

1 State Key Laboratory of Nonlinear Mechanics, Institute of Mechanics, Chinese Academy of Sciences, Beijing 100190, China

2 School of Engineering Science, University of Chinese Academy of Sciences, Beijing 100049, China

Vortex flow, as a typical feature in shear localization, is found not only in metallic glasses but also in other disordered materials, such as granular matter [29]. However, how does vortex evolve during the self-assembly of flow units? Moreover, what is the correlation between vortex evolution and macro-plasticity? These questions have so far remained elusive and need to be answered. Herein, a simple shear finite element model with two flow units embedded in the matrix was built to study the self-assembly of flow units in metallic glasses, especially the role of vortices in the percolation process. Our findings might have important significance for understanding the dynamics of the self-assembly of flow units and, consequently, for controlling shear band formation and propagation in metallic glasses and other disordered materials.

2 Theoretical Model

The interaction between two flow units in metallic glasses is analyzed by finite element simulations using ABAQUS. Since flow units are usually activated in regions with a relatively high free volume concentration [2, 30], we can distinguish the activated flow units from the surrounding material by assigning different free volume concentrations. Accordingly, the classical free volume model of metallic glasses is selected as the material constitutive model [31], which is coded as a UMAT subroutine and embedded in ABAQUS for calculation. The constitutive equations are expressed as follows.

The total strain rate $\dot{\varepsilon}_{ij}$ can be decomposed into elastic part $\dot{\varepsilon}^{\mathrm{e}}_{ij}$ and plastic part $\dot{\varepsilon}^{\mathrm{p}}_{ij}$, and is written as

$$\dot{\varepsilon}_{ij} = \dot{\varepsilon}^{\mathrm{e}}_{ij} + \dot{\varepsilon}^{\mathrm{p}}_{ij} \tag{1}$$

Due to the long-range atomic disorder, the elastic deformation of metallic glasses can be described by the generalized Hooke's law, that is

$$\dot{\varepsilon}^{\mathrm{e}}_{ij} = \frac{1+\upsilon}{E}\left(\dot{\sigma}_{ij} - \frac{\upsilon}{1+\upsilon}\dot{\sigma}_{kk}\delta_{ij}\right) \tag{2}$$

where E is Young's modulus; υ is Poisson's ratio. In addition to the elastic part, the plastic component $\dot{\varepsilon}^{\mathrm{p}}_{ij}$ is

$$\dot{\varepsilon}^{\mathrm{p}}_{ij} = \exp\left(-\frac{1}{\upsilon_{\mathrm{f}}}\right)\sinh\left(\frac{\sigma_{\mathrm{e}}}{\sigma_0}\right)\frac{S_{ij}}{\sigma_{\mathrm{e}}} \tag{3}$$

where $\upsilon_{\mathrm{f}} = \overline{\upsilon}_{\mathrm{f}} \big/ \alpha\upsilon^*$ is the normalized free volume, in which $\overline{\upsilon}_f$ is the average free volume per atom; α is a geometric factor of order 1; υ^* is the critical volume (hard-sphere volume of an atom); $S_{ij} = \sigma_{ij} - \sigma_{kk}\delta_{ij}/3$ is the deviatoric stress tensor; $\sigma_{\mathrm{e}} = \sqrt{\frac{3}{2}S_{ij}S_{ij}}$ is the effective stress; and $\sigma_0 = 2k_{\mathrm{B}}T \big/ \Omega$ is the reference stress, with k_{B} the Boltzmann constant, T the temperature, and Ω the atomic volume.

The evolution of free volume in the multiaxial stress state is expressed by Eq. (4), where free volume is created by squeezing an atom into an adjacent smaller vacancy and is annihilated by a series of diffusional atomic jumps.

$$\dot{\upsilon}_{\mathrm{f}} = \frac{1}{\alpha}\exp\left(-\frac{1}{\upsilon_{\mathrm{f}}}\right)\left\{\frac{\sigma_0}{S\beta\upsilon_{\mathrm{f}}}\left[\cosh\left(\frac{\sigma_{\mathrm{e}}}{\sigma_0}\right) - 1\right] - \frac{1}{n_{\mathrm{D}}}\right\} \tag{4}$$

where $\beta = \upsilon^* \big/ \Omega \sim 1$; $S = E/3(1-\upsilon)$; and n_{D} is the number of atomic jumps needed to annihilate a free volume equal to υ^*, which is generally taken as 3.

Relevant material parameters are given as $E = 96$ GPa, $\upsilon = 0.36$, $\alpha = 0.15$, and $\sigma_0 = 0.1$ GPa [32]. A rectangular sample with length $L = 3$ μm and width $W = 1$ μm is built. Two circular sections with radius $R = 50$ nm are created to represent the flow units (see Fig. 1). The whole sample contains a total number of around 1×10^4 plane strain elements. In order to ensure that the plastic deformation is confined to a single shear path, a stress concentration is introduced at the boundary of the specimen by setting a small notch. The notched sample is loaded by applying antisymmetric displacement boundary conditions on the two horizontal boundaries along the X-direction. Meanwhile, the movement in the Y-direction is constrained. The two vertical lines are free boundaries. Unless otherwise specified, the free volume concentration of the flow units is set as 0.1, while that of the surrounding material is 0.04, and the distance between the two flow units is $2R$.

3 Results and Discussion

Figure 2a shows the displacement vector field of the sample at $U = 0.013$ μm. Three vortices are observed in Fig. 2a, which are located in the middle between the two flow units as well as both the left and right sides of them. The clearer morphologies of the vortices marked in Fig. 2a are shown in Fig. 2b, as well the evolution of the vortices and free volume distribution with the loading displacement. From Fig. 2b, we can see that the vortices undergo three processes with the increase in displacement, from activation to growth, and to final collapse. We note that the evolution of the free volume around the flow units varies accordingly. When $U = 0.008$ μm, there is hardly any change in the free volume distribution, and no vortex has been found. When U reaches 0.014 μm, apparent free volume growth occurs between the flow units and vortices become visible. Then, with the further increase in vortex intensity, the content of free volume around the flow units keeps growing. At $U = 0.017$ μm, the matrix between the flow units has been greatly softened. The

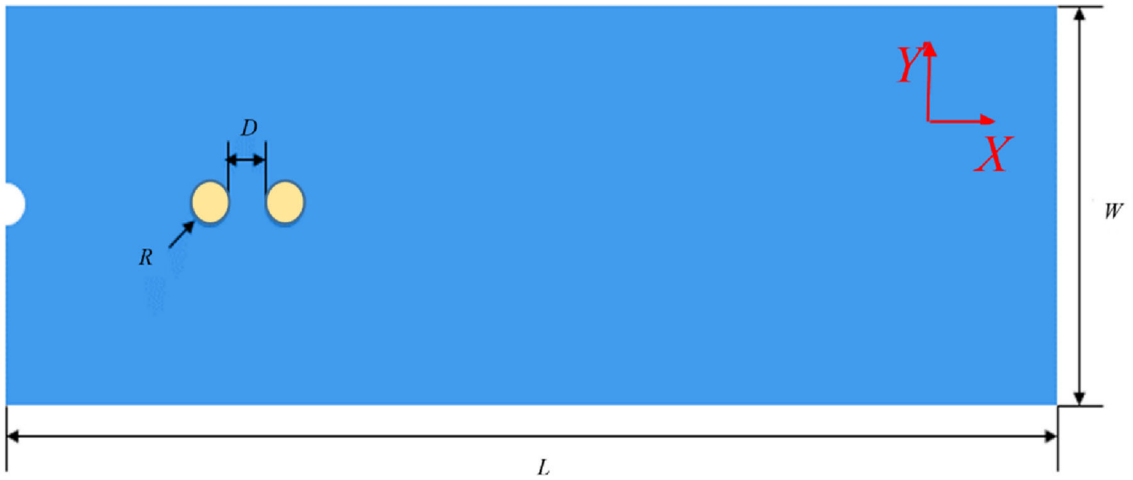

Fig. 1 Simple shear finite element model with two flow units embedded in the matrix

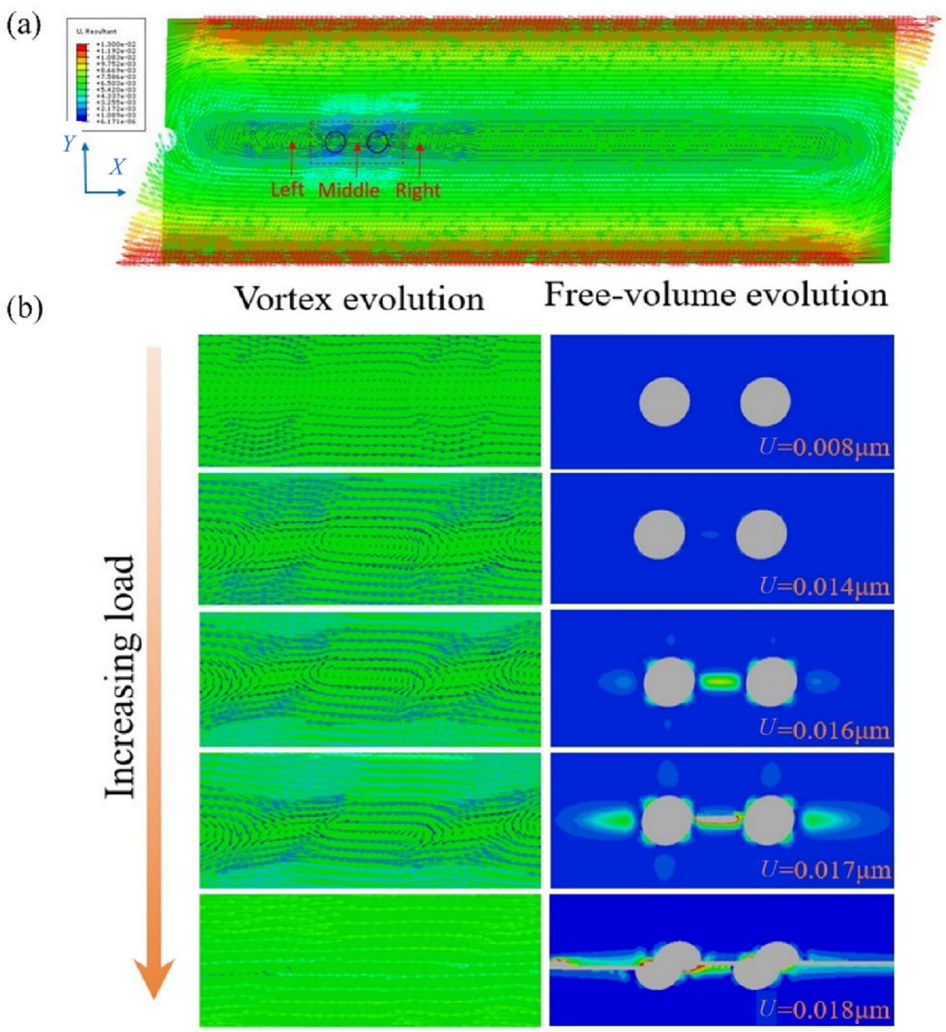

Fig. 2 **a** Displacement vector field of the sample at $U = 0.013$ μm; **b** the evolution of vortices and free volume concentration with the increase of external loading

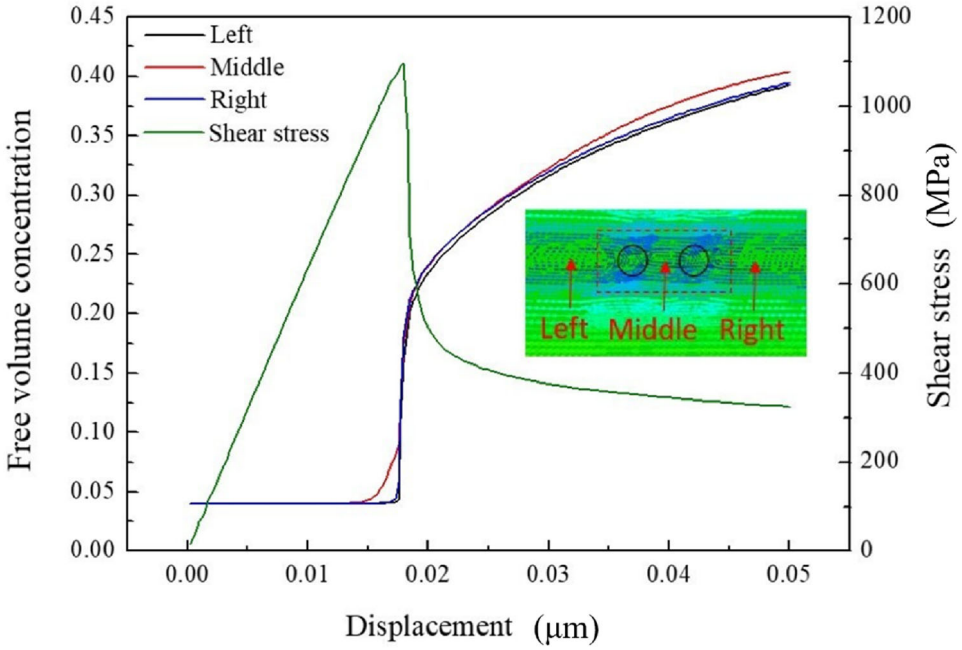

Fig. 3 Evolution curves of free volume concentration with loading displacement at the centers of the left, middle, and right vortices (as marked by the *inset*), and the macroscopic shear stress-displacement curve of the sample

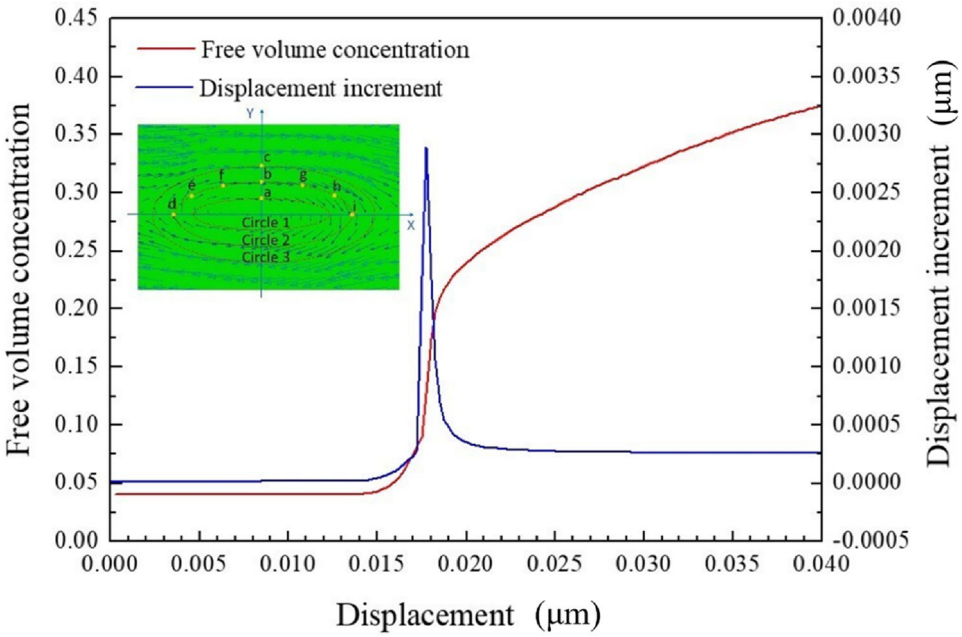

Fig. 4 Evolution curves of displacement increment at point b and free volume concentration at the middle vortex center with loading displacement

collapse of vortices occurs at $U = 0.018$ μm, and the percolation of flow units takes place, leading to a localized shear band.

To figure out the relationship between vortices, free volume, and macroscopic yielding, we plot the evolution curves of free volume concentration at the centers of three vortices with loading displacement and the macroscopic shear stress-displacement curve of the sample, which are displayed in Fig. 3. In comparison with those on the left and right sides, the free volume concentration at the center of the middle vortex goes up firstly at $U = 0.014$ μm. When it grows to a certain degree (close to 0.1), the free volume within the left and right vortices presents a sudden rise. At this point, the shear stress drops rapidly, causing the sample to yield.

As displayed by the inset of Fig. 4, three paths are defined, respectively, along circles 1, 2 and 3 from the core of the middle vortex to the outer shell, and the location points a-i are selected to study the evolution of deformation field before and after the vortex formation. The displacement increment at point b is calculated for each fixed time increment to represent the deformation velocity of the middle vortex, as shown in Fig. 4. Before the sample yields, the deformation velocity of

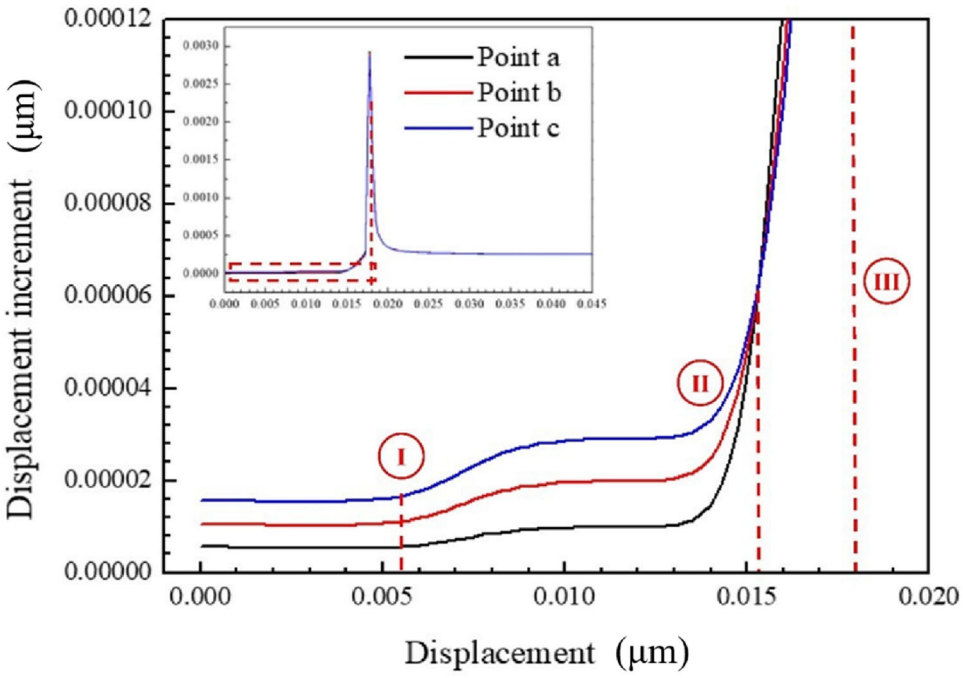

Fig. 5 Evolution curves of displacement increments at points a, b, and c, which are located in different circles

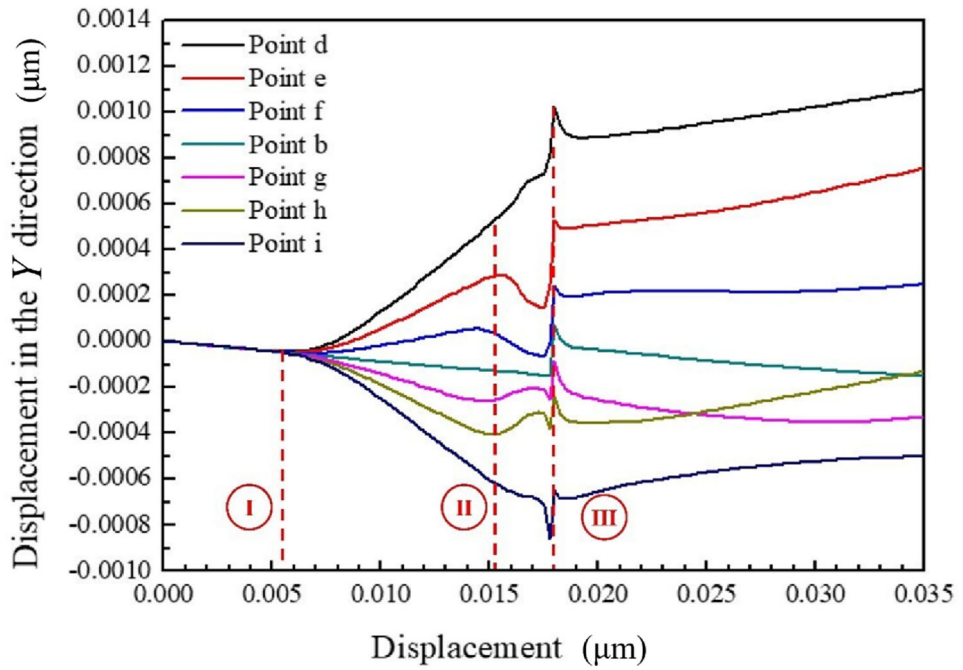

Fig. 6 Evolution curves of displacement in the *Y*-direction at different locations of the second circle

the vortex follows a similar trend to that of the free volume concentration: increasing obviously and changing suddenly at almost the same time, which indicates that the behavior of free volume is closely related to the evolution of vortices.

The evolution behavior of the vortex during deformation can be further described by Figs. 5 and 6. Choosing the middle vortex as an example, we can derive the variation of displacement increment at points a, b, and c, which are located in different circles (see Fig. 5). From the inset figure, we can see that the three curves overlap. The displacement increment first keeps constant, then undergoes a sharp increase and drop, and finally reaches a constant value larger than the initial. The enlarged figure shows a clear difference in the local area within the rectangle of the inset figure. Three characteristic points can be observed during the process, labeled I, II, and III. The displacement increment almost keeps constant during the initial period until *U* arrives at around 0.0055 μm (marked by I). From this point,

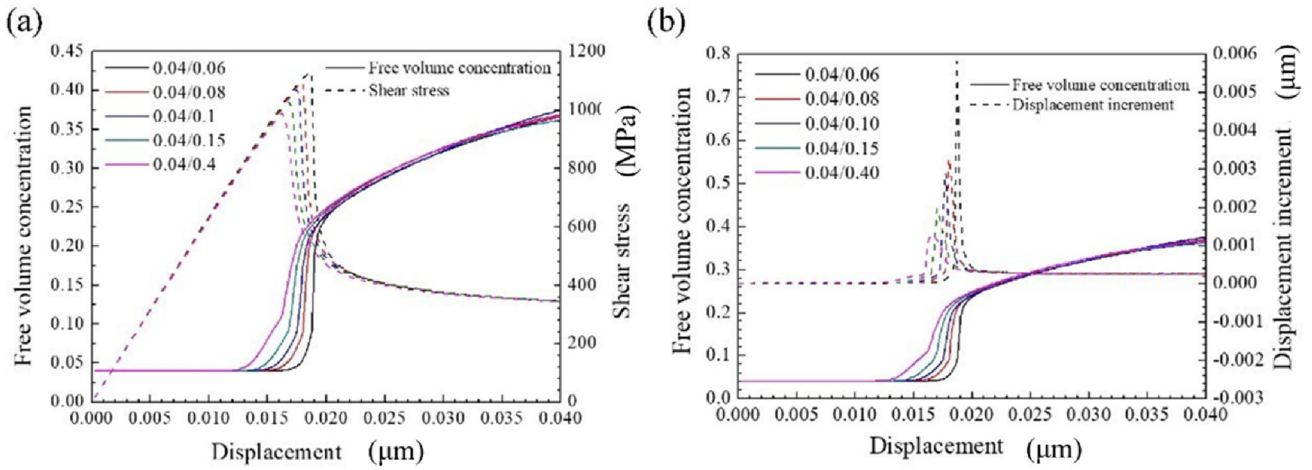

Fig. 7 **a** Evolution curves of free volume concentration with loading displacement at vortex centers and macro-shear stress-displacement curves of the samples; **b** the corresponding evolution curves of displacement increments at point b and free volume concentration for different initial free volume concentrations of flow units

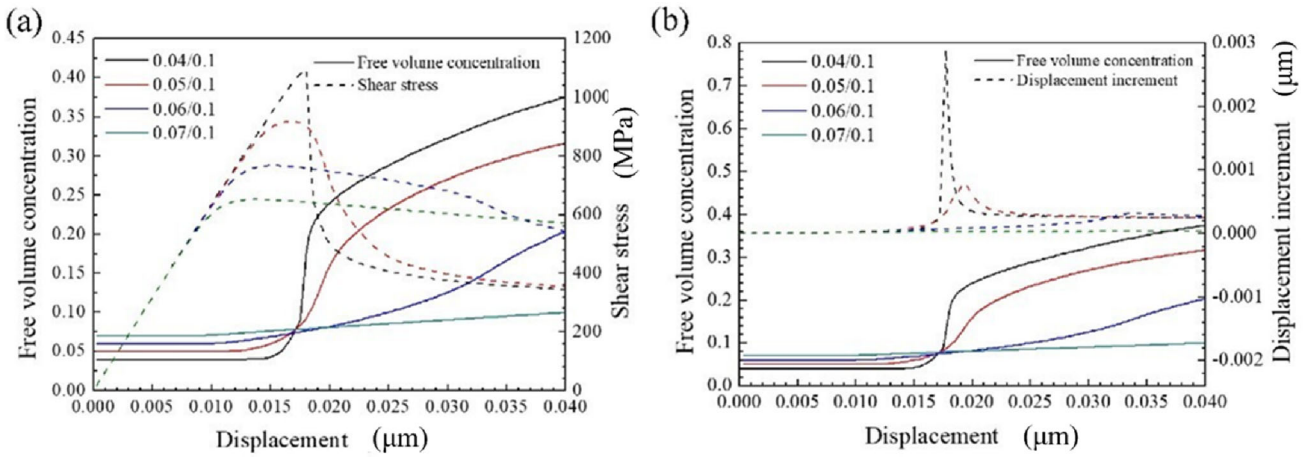

Fig. 8 **a** Evolution curves of free volume concentration with loading displacement at vortex center and macro-shear stress-displacement curves of the samples; **b** the corresponding evolution curves of displacement increment at point b and free volume concentration for different initial free volume concentrations of matrix

the displacement increment grows slowly. Accordingly, the displacement in the Y-direction at different places of the second circle is displayed by Fig. 6. Since the displacement applied to the sample is along the X-direction, the material points initially have the same Y-direction displacement around zero. A bifurcation starts from I, where the location points d-f and g-i exhibit opposite deflections, suggesting that the deformation field experiences a rotation. This could be an indicator of the activation of vortex flow, even though a visible vortex is still hardly captured at $U = 0.008$ μm (see Fig. 1b).

The displacement increment increases gradually from the core of the vortex to the periphery. When $U = 0.014$ μm, the displacement increment shifts from a smooth change to a sharp one. At transition point II, the displacement increments for three locations a-c reach the same value (see Fig. 5). A transition is also observed in the evolution of the Y-direction displacement (see Fig. 6), and the magnitude of the Y-direction displacement changes from an increase to a decline. This indicates that the vortex, which is activated at I, develops into its mature stage at II, and then weakens. The displacement increment reaches its maximum labeled by III and then falls rapidly, and correspondingly, the Y-direction displacement has a sudden rise for all location points and the symmetrical deflection trend is broken. It suggests that the vortex collapses and the percolation of flow units takes place.

The initial free volume concentration has been identified as an important factor influencing shear band formation and

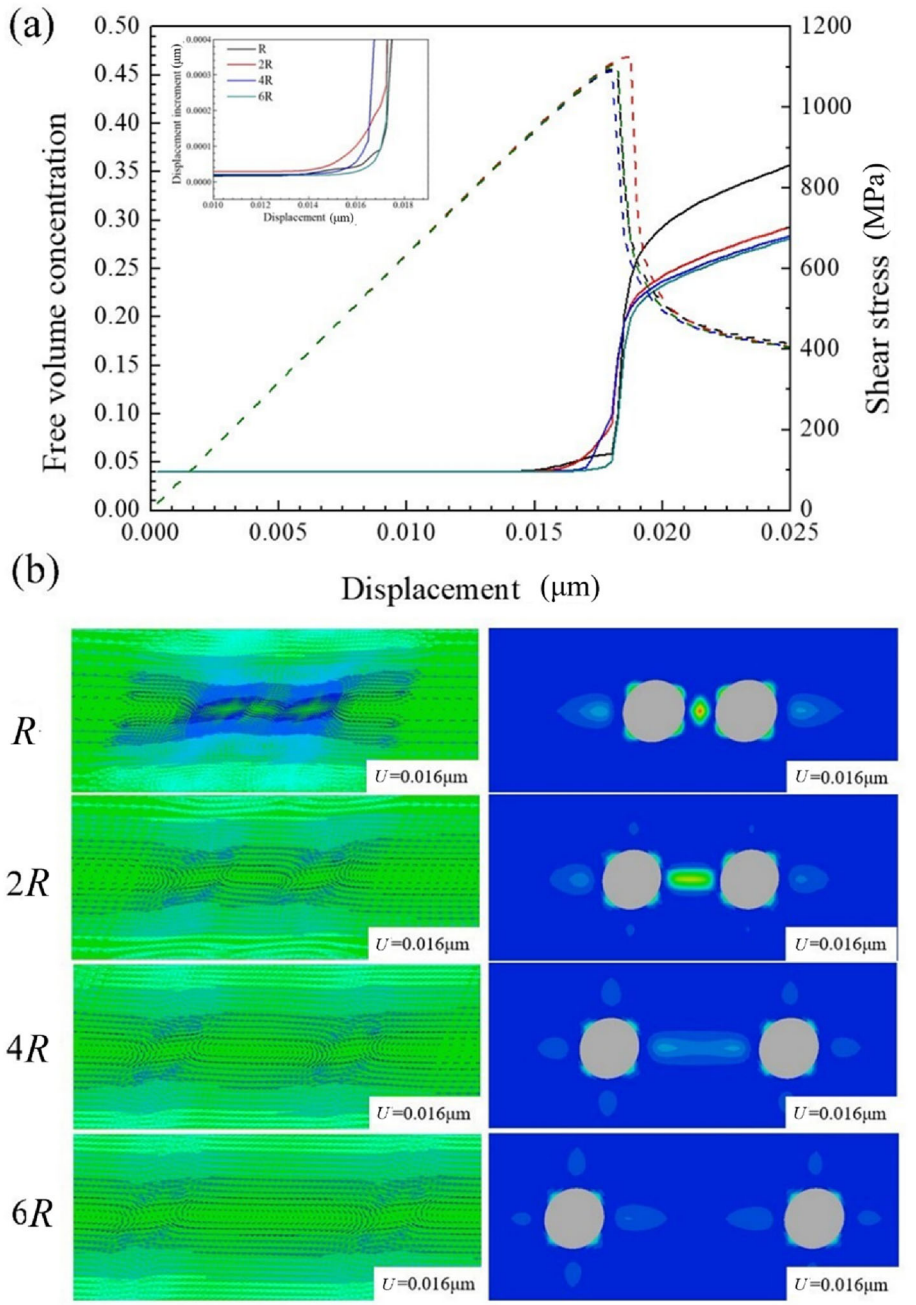

Fig. 9 **a** Evolution curves of free volume concentration with loading displacement and macro-shear stress-displacement curves of samples with varied spacing of flow units; **b** the shapes of vortices and free volume distributions at $U = 0.016$ μm for varied spacing of flow units

multiplication [8]. How does the initial free volume affect the vortex evolution? We change the initial free volume concentrations of the flow units and the surrounding matrix, respectively, in the simulation. In Fig. 7, the initial free volume concentration of the matrix is kept constant at 0.04, while the initial free volume concentration of the flow units is varied from 0.06 to 0.4. We can see that with the increase of initial free volume concentration of the flow units, the free volume concentration within the middle vortex starts to grow earlier, and correspondingly, the whole sample yields at a smaller loading displacement with a lower shear stress (see Fig. 7a). It is seen from Fig. 7b that a larger initial free volume concentration of the flow units also leads to earlier activation and a more gentle evolution process of the vortex. The peak value of displacement increment at point b increases with the decrease in initial free volume concentration, corresponding to a high evolution speed of the vortex. The formation of a mature vortex, which corresponds to a considerable production of free volume, suggests a transition from elastic deformation to plastic deformation, and the breakdown of vortex indicates that flow units percolate to each other and

a shear band forms. Therefore, the vortex evolution process from II to III dominates homogeneous plastic deformation.

If the initial free volume concentration of flow units remains unchanged, while that of the surrounding matrix varies from 0.04 to 0.07, as shown in Fig. 8, the evolution of free volume slows down and the overshoot of the shear stress-displacement curves tends to be less obvious (Fig. 8a). A similar phenomenon can also be observed from the evolution curves of displacement increment in Fig. 8b. With the growth of the initial free volume concentration within the matrix, the vortex evolves more slowly and tenderly, and the peak even disappears. This indicates that a higher initial free volume concentration will result in better homogeneous plasticity. In this sense, we can speculate a brittle-to-ductile transition of metallic glasses from their vortex evolution behavior.

The effect of the distance D between two flow units on the deformation behavior is shown in Fig. 9. With the distance D varying from R to $6R$, the yield stress of the sample initially increases and then decreases. When the spacing is $2R$, the yield stress is highest. A similar non-monotonic trend can be found in the evolution curves of free volume concentration and displacement increment, as shown in Fig. 9a. This phenomenon indicates that there exists optimal spacing near $2R$ to maximize the strength of the material. The vortex morphology for varied spacing at $U = 0.016$ μm is displayed in Fig. 9b. The shape of the vortex tends to be "flatter" with the increase in spacing. Accordingly, the free volume distribution shows that the interaction of flow units becomes weaker as the spacing increases.

4 Conclusions

The activation, growth and collapse behavior of vortices during the self-assembly of flow units in metallic glasses was investigated through simulations. It was found that the formation of a mature vortex indicates the onset of yielding, and the collapse of the vortex represents the percolation of flow units or shear localization. The vortex evolution behavior depends on the initial free volume distribution and the spacing of flow units. Generally, increasing the initial free volume concentration within flow units or the matrix leads to a gentler vortex evolution process and better homogeneous plasticity. The shape of the vortex tends to be "flatter" with the increase in flow units' spacing, and the optimal spacing was found to maximize the strength of the material. These results may shed light on the detailed process of self-assembly of flow units in metallic glasses from vortex evolution. Furthermore, they suggest a potential way to manipulate the self-assembly of flow units by regulating the vortex evolution behavior properly and, ultimately, to improve the plastic deformability of metallic glasses.

Acknowledgements This work is supported by the NSFC (Nos. 11972346 and 11790292), and the NSFC Basic Science Center Program for "Multi-scale Problems in Nonlinear Mechanics" (No. 11988102).

Author's Contributions JL contributed to simulation and writing—original draft. RS contributed to simulation and writing—original draft. YC contributed to conceptualization, analyses, supervision, and writing—original draft, review and editing. LD contributed to writing—review and editing.

Declarations

Conflict of interest The authors declare no conflict of interest.

Consent for Publication All authors approved the final manuscript and the submission to this journal.

References

1. Argon AS. Plastic deformation in metallic glasses. Acta Metall. 1979;27:47–58.
2. Falk ML, Langer JS. Dynamics of viscoplastic deformation in amorphous solids. Phys Rev E. 1998;57(6):7192–205.
3. Wang WH. The elastic properties, elastic models and elastic perspectives of metallic glasses. Prog Mater Sci. 2012;57(3):487–656.
4. Falk ML Langer JS, Chen Y Trans, Wang YJ Proof, Deformation and failure of amorphous, solidlike materials. Advances in Mechanics. 2021;51(2): 406–26.
5. Liu YH, Wang G, Wang RJ, Zhao DQ, Pan MX, Wang WH. Super plastic bulk metallic glasses at room temperature. Science. 2007;315(5817):1385–8.
6. Liu YH, Wang D, Nakajima K, Zhang W, Hirata A, Nishi T, Inoue A, Chen MW. Characterization of nanoscale mechanical heterogeneity in a metallic glass by dynamic force microscopy. Phys Rev Lett. 2011;106(12): 125504.
7. Tian ZL, Wang YJ, Chen Y, Dai LH. Strain gradient drives shear banding in metallic glasses. Phys Rev B. 2017;96(9): 094103.
8. Chen Y, Jiang MQ, Dai LH. How does the initial free volume distribution affect shear band formation in metallic glass? Sci China Phys Mech Astron. 2011;54(8):1488–94.
9. Qiao JC, Wang Q, Pelletier JM, Kato H, Casalini R, Crespo D, Pineda E, Yao Y, Yang Y. Structural heterogeneities and mechanical behavior of amorphous alloys. Prog Mater Sci. 2019;104:250–329.
10. Zhang M, Chen Y, Li W. On the origin of softening in the plastic deformation of metallic glasses. Int J Plastic. 2019;116: 24–38.
11. Qian JC, Zhang LT, Tong Y, Lyu GJ, Hao Q, Tao K. Mechancial properties of amorphous alloys: In the framework of the microstructure heterogeneity. Adv Mech. 2022;51(1):117–52.
12. Schuh CA, Lund AC. Atomistic basis for the plastic yield criterion of metallic glass. Nat Mater. 2003;2(7):449–52.
13. Şopu D, Stukowski A, Stoica M, Scudino S. Atomic-level processes of shear band nucleation in metallic glasses. Phys Rev Lett. 2017;119(19): 195503.
14. Chen Y, Dai L. Failure behavior and criteria of metallic glasses. Acta Mech Sin. 2022;38: 121449.
15. Wang Z, Wen P, Huo LS, Bai HY, Wang WH. Signature of viscous flow units in apparent elastic regime of metallic glasses. Appl Phys Lett. 2012;101(12): 121906.
16. Yang ZY, Wang YJ, Dai LH. Hidden spatiotemporal sequence in transition to shear band in amorphous solids. Phys Rev Res. 2022;4(2):023220.
17. Jiang MQ, Wang WH, Dai LH. Prediction of shear-band thickness in metallic glasses. Scripta Mater. 2009;60(11):1004–7.

18. Zhang Y, Greer AL. Thickness of shear bands in metallic glasses. Appl Phys Lett. 2006;89(7): 071907.
19. Greer AL, Cheng YQ, Ma E. Shear bands in metallic glasses. Mater Sci Eng R. 2013;74(4):71–132.
20. Sunny G, Yuan F, Prakash V, Lewandowski J. Design of inserts for split-hopkinson pressure bar testing of low strain-to-failure materials. Exp Mech. 2008;49(4):479–90.
21. Bulatov VV, Argon AS. A stochastic model for continuum elasto-plastic behavior: I. Numerical approach and strain localization. Modell Simulat Mater Sci Eng. 1994;2: 167–84.
22. Lemaitre A, Caroli C. Rate-dependent avalanche size in athermally sheared amorphous solids. Phys Rev Lett. 2009;103(6):065501.
23. Scudino S, Şopu D. Strain distribution across an individual shear band in real and simulated metallic glasses. Nano Lett. 2018;18(2):1221–7.
24. Hieronymus-Schmidt V, Rösner H, Wilde G, Zaccone A. Shear banding in metallic glasses described by alignments of Eshelby quadrupoles. Phys Rev B. 2017;95(13): 134111.
25. Jiang MQ, Dai LH. On the origin of shear banding instability in metallic glasses. J Mech Phys Solids. 2009;57(8):1267–92.
26. Chen Y, Jiang MQ, Dai LH. Collective evolution dynamics of multiple shear bands in bulk metallic glasses. Int J Plast. 2013;50:18–36.
27. Dai LH. Shear banding in bulk metallic glasses. In: Dodd B, Bai YL, editors. Adiabatic shear localization: frontiers and advances. London: Elsevier; 2012. p. 311–61.
28. Lu H, Tang Y, Jiang F, Wan P, Zhou H. mechanical properties and deformation mechanisms of metallic glasses under hydrostatic pressure. Acta Mech Solida Sin. 2023. https://doi.org/10.1007/s10338-023-00390-3.
29. Padbidri JM, Hansen CM, Mesarovic SD, Muhunthan B. Length scale for transmission of rotations in dense granular materials. J Appl Mech. 2012;79(3): 031011.
30. Ding G, Jiang F, Dai L, Jiang M. Effective energy density of glass rejuvenation. Acta Mech Solida Sin. 2022;35(5):746–54.
31. Spaepen F. A microscopic mechanism for steady state inhomogeneous flow in metallic glasses. Acta Metall. 1977;25:407–15.
32. Gao YF. An implicit finite element method for simulating inhomogeneous deformation and shear bands of amorphous alloys based on the free-volume model. Modell Simulat Mater Sci Eng. 2006;14(8):1329–45.